Speed-of-sound imaging in a photoacoustic imager

Srirang Manohar,[a,*] René G. H. Willemink,[b] and Ton G. van Leeuwen[a]

[a] Institute for Biomedical Technology (BMTI), Biophysical Engineering Group, Faculty of Applied Physics (TNW), University of Twente, Postbox 217, 7500AE Enschede, The Netherlands

[b] Institute for Biomedical Technology (BMTI), Signals and Systems Group (SaS), Faculty of Electrical Engineering (EWI), University of Twente, Postbox 217, 7500AE Enschede, The Netherlands

ABSTRACT

The effects of an inappropriately chosen speed-of-sound in photoacoustic imaging reconstructions are to cause blurring of images and impairment of contrast. Here we outline a new methodology to measure the speed-of-sound in a photoacoustic imager with little or no additional cost and without the need to perform extra measurements. The method uses a strong absorber of light which is placed in the path of the light illuminating the sample. This acts as a source of ultrasound whose interaction with the sample can be measured at the far-end of the sample using the same ultrasound detector used for photoacoustics. This yields time-of-arrival measurements of the ultrasound transient at the multi-element detector. Such measurements are made at various angles around the sample in a computerized tomography approach. Reconstruction of the time-of-arrival or speed-of-sound tomogram of the object can be made by implementing a fan-beam projection reconstruction algorithm. We present the concept and validate the method on a speed-of-sound phantom.

1. INTRODUCTION

Photoacoustic imaging is a relatively new non-invasive imaging technique that has utility in the visualization of absorbing structures in soft tissue.[1] Photoacoustics has applications in the detection of cancer in the human breast ,[2–4] depicting of blood vessels for diagnosis in humans[5,6] and in small-animal imaging[7–9] for fundamental studies connected with visualizing vascularization and angiogenesis associated with cancer growth. The technique combines the advantages of high optical absorption contrast presented by chromophores present in blood, with the high resolution that is a consequence of low ultrasound scattering in soft tissue.

The principle of the photoacoustic effect involves the localized emission of heat as a consequence of non-radiative deexcitation of absorbed light. The resulting temperature rise cause thermal expansion and when pulsed light is used for excitation, pressure transients are created which propagate through the tissue to be recorded by ultrasound detectors at the surface of the tissue. An imager consists of pulsed light excitation in the near-infrared wavelength region which provides deep penetration of light in tissue, with multi-element or multi-position ultrasound detection. Ultrasound transients recorded at different locations enable a localization of the acoustic source and thereby the optical absorber by knowing or assuming a speed-of-sound (SOS) in the medium. The choice of SOS thus has implications in determining the exact location of absorbers excited by the photoacoustic effect. Choosing an appropriate speed-of-sound (SOS) is not trivial since it is well know that tissue possesses a spectrum of velocities ranging from 1350 m/s for fat to 1700 m/s for skin.[10]

Recently there have been a few methods that have enabled the measurement of SOS using photoacoustic imaging.[11,12] However these methods may be improved upon. In this article we present a simple method that enables the measurement of the SOS in objects that are under photoacoustic investigation, allowing tomograms of the spatial distribution of acoustic velocity to be made.

* Author for correspondence: S.Manohar@utwente.nl

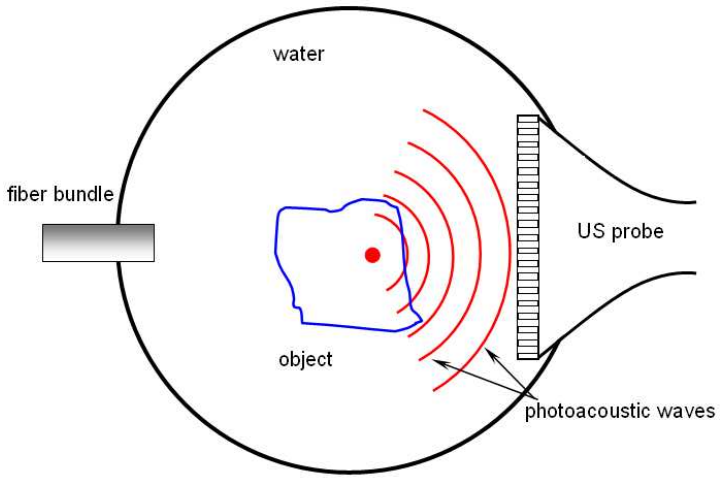

Figure 1: Schematic of a computerized Photoacoustic imager.

2. REQUIREMENTS FOR SPEED-OF-SOUND MEASUREMENTS IN PHOTOACOUSTICS

Figure 1 shows the schematic of a typical computerized tomography (CT) photoacoustic (PA) imager. The object under investigation is mounted on a rotary stage to be suspended in water in an imaging tank. The fiber bundle transports pulsed near-infrared (NIR) light to illuminate the object. At the far end a linear ultrasound (US) probe is positioned. Ultrasound produced in the object by the PA effect, propagates through the water to be recorded by the detector elements; this is a projection The object is then rotated in angular steps covering 360^o recording projections at each angle.

Reconstruction of the acoustic source distribution or PA image of the object is performed using various modifications of filtered backprojection.[13–15] The difference between backprojection performed in this case and that used in x-ray CT imaging is that in the latter the backprojection is performed along straight line paths. In photoacoustics as in ultrasound transmission computed tomography (UTCT), backprojection is performed along

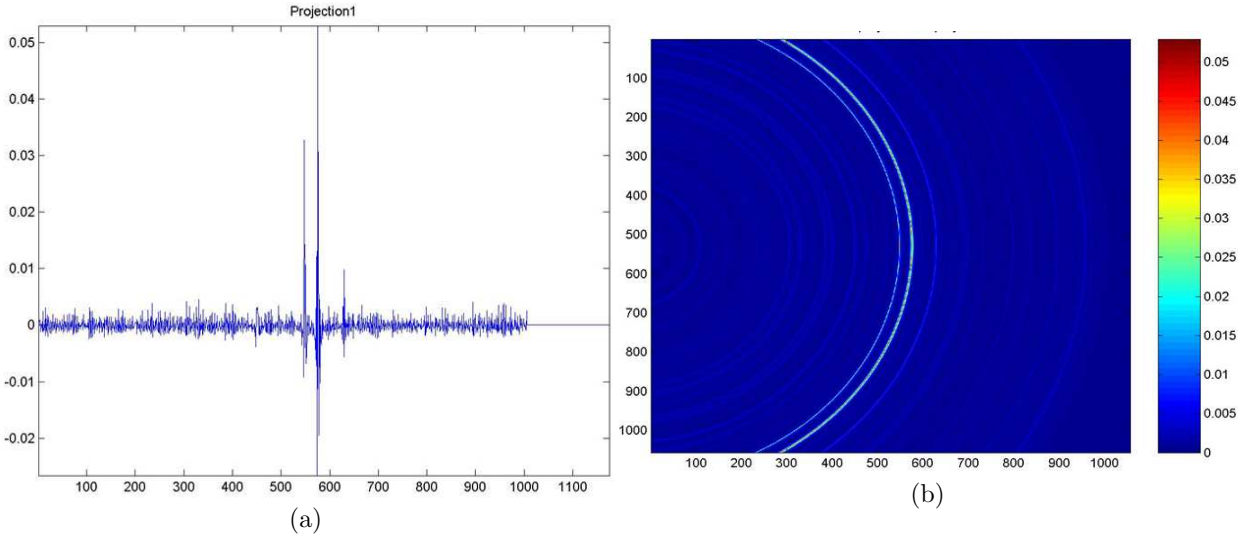

Figure 2: (a) A-scan or photoacoustic projection of an object at a single angle. (b) Backprojection of the signal into image space. Integrating over all angles allows the object function to be reconstructed.

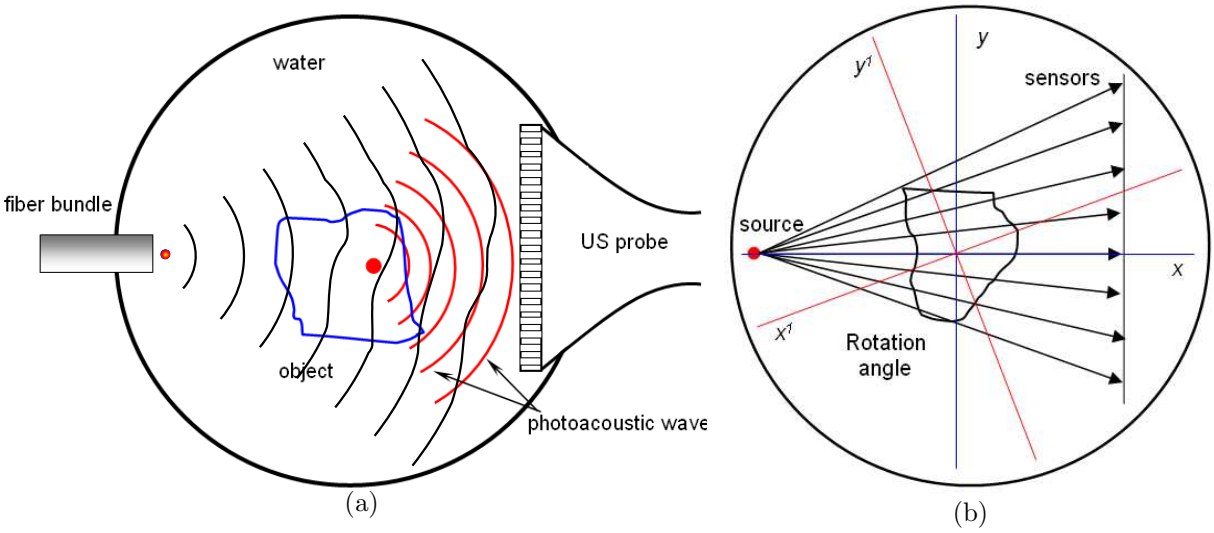

Figure 3: (a) Concept for speed-of-sound imaging using photoacoustics by introducing a carbon-fiber at the position of illumination. (b) Fan-beam reconstruction geometry applicable for generating speed-of-sound images.

circular paths and may be termed acoustic backprojection.[16] Figure 2(a) is a real A-scan of a phantom carrying absorbing structures and Fig. 2(b) shows the smearing out of the signal trace in half-circles into image space. Integrating over all angles results in a constructive interference of signals where an acoustic source is present resulting in a reconstruction of the PA image. In this reconstruction it is implicit that the time-axis of the signal trace is translated into a distance-axis by multiplying it with the SOS of the object and coupling medium.

There are two assumptions that are inherent to acoustic backprojection:

1. The acoustic velocity of the object is known,
2. The object is acoustically homogeneous.

In general these 2 assumptions are invalid in tissue. In most cases, the SOS of the object is not measured, rather a typical value is used in the reconstruction based on values published in the literature. Also a single SOS is chosen for the entire object contrary to the knowledge that acoustic velocities are dependent on tissue types, which would imply a spatial SOS distribution in the object. The result of these 2 assumptions is that there is no guarantee that the acoustic backprojections will overlap which would lead to a compromised resolution and poor contrast.

If instead of choosing a single SOS value for the object, the real SOS distribution in the object was measured then this could be used to correct the acoustic backprojection paths to undergo distortions to the perfect circular paths based on the spatial inhomogeneities in SOS. While 2 methods have been recently proposed to measure the SOS, both can be improved upon. The method of Kolkman *et al*[11] requires the presence of well-defined absorbers in the tissue which is in general not the case. The method of Jin and Wang[12] requires a separate ultrasound transmitter and necessitates an extra measurement in addition to the conventional PA protocol.

3. A NEW METHODOLOGY FOR SPEED-OF-SOUND IMAGING

The proposed method makes use of the photoacoustic effect to generate a reference acoustic pulse which interacts with the object permitting the SOS to be measured. Figure 3(a) shows the scheme of the method. A carbon fiber is positioned in the imaging tank in front of the fiber bundle to be in the path of light illuminating the object. The carbon fiber absorbs the light incident on it strongly setting up an ultrasound transient by the photoacoustic effect. The carbon fiber ensure that the acoustic waves which are produced fan out in the imaging

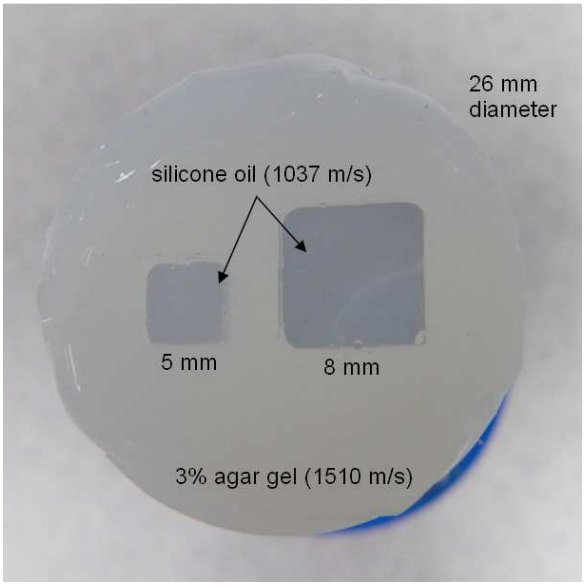

Figure 4: Photograph of the phantom used for demonstrating the concept of speed-of-sound imaging. Two square cross-sectional cavities are made in an agar gel cylinder. The cavities are filled with silicone oil and sealed. The speed-of-sound values of the different materials are indicated.

plane but are restricted in the plane orthogonal to this. The otherwise circular wavefront is distorted as the wave interacts with the object. Where regions of higher acoustic velocity are encountered there is an advancement of the wavefront; retardation of the wavefront occurs when regions of lower SOS are encountered. The pulse propagates through the object to be collected at the far-end by the individual elements of the ultrasound probe. The times-of-arrival (TOA) of the pulse can then be easily extracted at each element.

Instead of measuring the TOA directly, a reference measurement can be made retracting the object, allowing the ultrasound to propagate in water alone. In such a case undistorted circular wavefronts can be expected which are then recorded at each element. A cross-correlation between segments of a signal trace carrying the ultrasound transient, with and without the object, then provides information of the SOS changes with and without the sample in water.

Simultaneously, since the cross-section of the carbon fiber is small, a major portion of the light illuminates the object setting up ultrasound from absorbing structures inside the object. This is recorded in the same signal trace as the transient from the carbon fiber, only the two sets of signals are separated in time. The same signal trace of an element now possesses information regarding the SOS of the object but also conventional photoacoustically relevant information from the object.

In a first approximation, the TOA or TOA difference of a pulse at a certain detector is inversely proportional to the integrated SOS between the carbon fiber and the detector element considered. For all the elements at a certain projection, the situation is comparable to a fan-beam geometry which is used in x-ray CT imaging. This is shown in Fig. 3(b). A CT type experiment is then performed rotating the object in angular steps to cover 360°. A TOA or TOA difference image may be then recovered by applying the conventional inverse Radon transform in the fan-beam geometry.[17] This tomogram can be translated into a SOS image (or SOS difference image if TOA difference data is used) with a knowledge of the dimensions of the geometry such as distance between the detector and the carbon fiber. Alternatively, a knowledge of the SOS in water would allow the SOS difference image to be modified to yield the absolute SOS image of the object.

4. MATERIALS AND METHODS

A simple phantom was created to test the above hypothesis. In a cylindrical mould, two square cross-section brass bars of side 5 mm and 8 mm respectively were suspended. Three percent agar was dissolved in water at

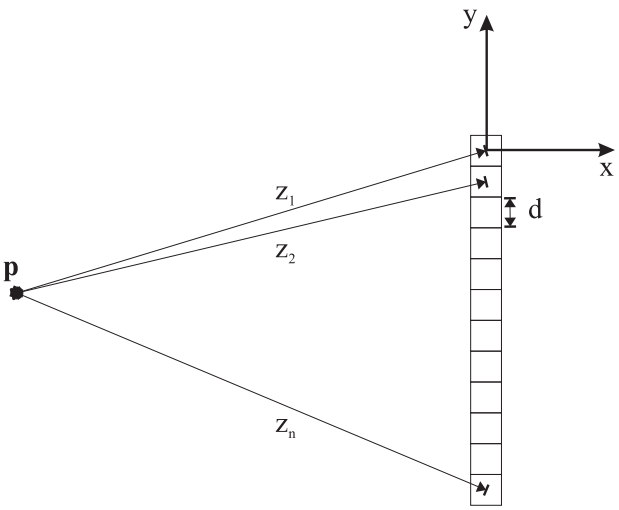

Figure 5: Geometry of system for speed-of-sound estimation. The location of the carbon-fiber is at p; the linear detector with inter-element spacing d array is at the far end.

95°C poured in to the mould and allowed to set. The brass bars were carefully removed when the solution had gelled to leave an agar gel cylinder of 26 mm diameter with 2 cavities. A schematic of the phantom in top view is shown in Fig. 4. The cavities were filled with silicone oil and then sealed. The SOS of 3% agar gel block was measured using the insertion method[10] to be 1510 m/s. The SOS of the oil was measured to be 1037 m/s.

The phantom was mounted on a rotary stage and suspended in an imaging tank filled with water. The tank had a 128 element ultrasound detector inserted through an aperture. Opposite to the ultrasound probe was a fiber bundle inserted through an aperture. A carbon fiber of 250μm was mounted at the end of the bundle at a distance of 5 mm from its face. Light from an Nd:YAG laser was made to illuminate the carbon fiber and SOS phantom. Signals were recorded from each element of the probe for 60 angle around 360°.

The phantom was then retracted and a reference measurement was performed in water alone at a single angle, with signals measured from all the elements. The carbon fiber transients from phantom and water measurement were cross-correlated and the TOA differences with and without phantom in water were estimated. The data was then used to perform an inverse Radon transform in fan-beam geometry using the Matlab 7.04 (The MathWorks, Inc., Natick,MA) function *ifanbeam*.

5. RESULTS

From the reference measurement the SOS in water was calculated to be 1490 m/s as expected. This was obtained by fitting the TOA of the carbon-fiber pulses at each element of the US probe to a model which was based on the geometry of the experiment. The fit included SOS in water, and dimensional parameters such position of the carbon-fiber with respect to the detector array (See Fig. 5) along x and y, and the interelement spacing of the detector which was fixed at 320 μm. From the measured SOS in water, it may be concluded that any non-linear propagation effects of the ultrasound through water for the pressure intensities created at the carbon fiber are insignificant if not non-existent.

Figure 6 shows the TOA difference tomogram, and Fig. 7(a) shows the corresponding SOS image. It is seen in both images that the oil filled cavities in the agar background have been clearly depicted. In Fig. 7(a) sampling the low SOS regions at various locations yields an average SOS around 1100 m/s which is close to the 1037 m/s measured independently for the silicone oil. Figure 7(b) shows the intensity profile along the line superposed on the SOS image; the variations in SOS due to the oil in the cavities is clearly seen. Also marked in Fig. 7(b) are the values corresponding to the oil and the background agar (1520 m/s).

There are however artifacts that are present as high SOS clutter in the background. While more investigations need to be performed and various experimental and analysis aspects need to be fine tuned, the reason for the

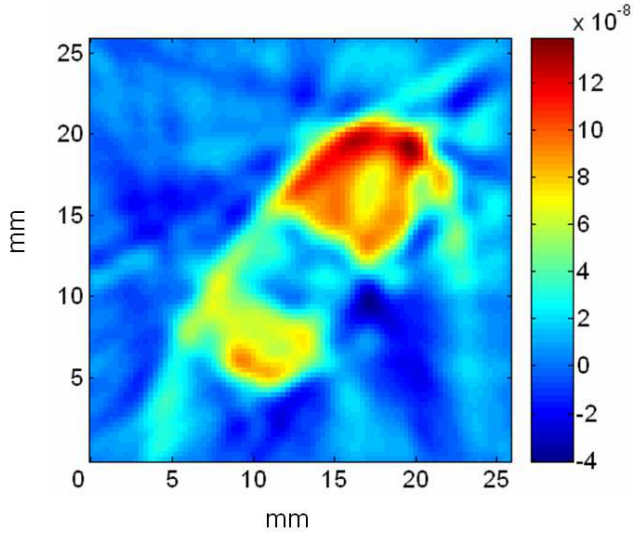

Figure 6: Time-of-arrival tomogram of the phantom reconstructed using a fan-beam tomography algorithm using times-of-arrival of acoustic pulses generated by the carbon-fiber.

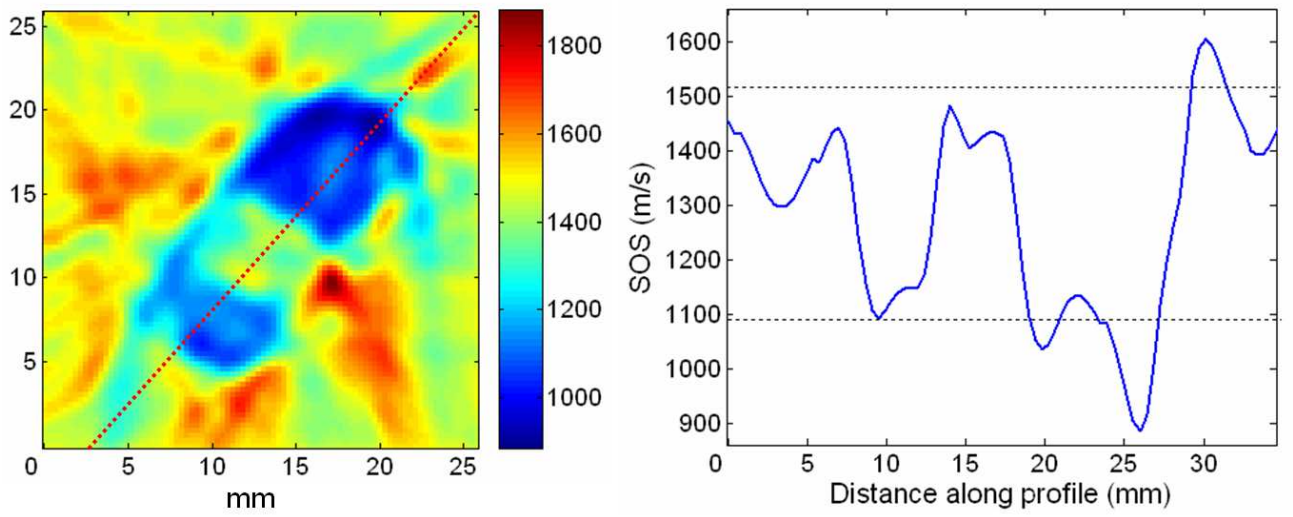

Figure 7: (a) Speed-of-sound tomogram of the phantom reconstructed using a fan-beam tomography algorithm using times-of-arrival of acoustic pulses generated by the carbon-fiber. An intensity profile is made through the dotted line in the image. (b) Profile of intensities encountered along the line through the speed-of-sound image of the phantom. Marked on the graph are values of 1037 m/s and 1520 m/s which are expected for the oil and surrounding agar in the phantom.

artifacts may be due to strong refraction that occurs at the interface of the agar and oil; the refractive index of the oil referenced to the agar is 0.7. This will cause severe refraction and deviation of the rays emanating from the carbon fiber away from the line of sight.

6. DISCUSSION

The hypothesis of using the ultrasound pulses generated by a strong absorber located in the path of illuminating light to measure SOS of the object is valid. In a simple phantom we have been able to image the SOS inhomogeneities with numerical values in the image broadly matching independently measured SOS values of the materials used in the phantom. The images however have artifacts the origin of which are possibly due to the high mismatch in acoustic impedances at the interfaces which causes bending of the rays; the imaging algorithm explicitly assumes straight line paths from source to detector. We will investigate this technique further and concentrate on SOS phantoms which have smaller SOS contrast compared with the background. These contrasts will be brought down to physiological values which are typically present in tissue. In such a situation it is likely that the artifacts will disappear. In any case, we will also implement an algorithm which can deal with bent rays. A candidate algorithm is already under study which will enable true SOS images or true refractive index images to be reconstructed. This is based on an iterative approach considering acoustical ray tracing through an initial SOS tomogram following Snell's law and using this to generate corrected SOS images.

No absorbers were introduced in the phantom in these preliminary studies. This is planned in the near future where we will measure the photoacoustic signals from the object as well as spatial variations in the SOS. These SOS distributions will be used to correct the backprojection paths. The correction method of Jing and Wan[12] appears attractive to implement.

The use of the carbon fiber as ultrasound transmitter makes the method simple, inexpensive and convenient. No extra measurements need to be performed with this approach. Though a carbon fiber of 250μm has been used in this work, there is no restriction to the type of material, the geometry or number of structures used. Different materials such as black human hair, colored nylon thread or gold nanostructures embedded in a suitable transparent substrate may be used. Spherical absorbers may also be used as point sources if a measurement in a hemispherical or cylindrical geometry in 3 dimensions is required.

ACKNOWLEDGMENTS

This research is supported by a personal grant to S. Manohar in the Vernieuwingsimpuls program (Veni) by the Nederlandse Wetenschappelijk Organisatie (NWO) and Stichting Technische Wetenschappen (STW). Authors are also grateful to the Institute for Biomedical Technology (BMTI) of the University of Twente for funding in the NIMTIK program.

REFERENCES

1. M. Xu and L. V. Wang, "Photoacoustic imaging in biomedicine," *Rev. Sci. Instrum.* **77**(04110), 2006.
2. A. A. Oraevsky, E. V. Savateeva, S. V. Solomatin, A. A. Karabutov, V. G. Andreev, Z. Gatalica, T. Khamapirad, and P. M. Henrichs, "Optoacoustic imaging of blood for visualization and diagnostics of breast cancer," in *Biomedical Optoacoustics III*, A. A. Oraevsky, ed., *Proc. Soc. Photo-Opt. Instrum. Engg. (SPIE)* **4618**, pp. 81–94, 2002.
3. R. A. Kruger, K. Stantz, and W. L. Kiser Jr., "Thermoacoustic CT of the breast," in *Physics of Biomedical Imaging*, L. E. Antonuk and M. J. Jaffe, eds., *Proc. (SPIE)* **4682**, pp. 521–5, 2002.
4. S. Manohar, A. Kharine, J. G. C. van Hespen, W. Steenbergen, and A. G. C. van Leeuwen, "The Twente Photoacoustic Mammoscope: system overview and performance," *Phys. Med. Biol.* **50**, pp. 2543–57, 2005.
5. R. G. M. Kolkman, E. Hondebrink, W. Steenbergen, and F. F. M. de Mul, "*In vivo* photoacoustic imaging of blood vessels using an extreme-narrow aperture sensor," *IEEE J. Sel. Topics Quant. Electron.* **9**, pp. 343–6, 2003.
6. H. F. Zhang, K. Maslov, G. Stoica, and L.-H. Wang, "Functional photoacoustic microscopy for high-resolution and noninvasive *in vivo* imaging," *Nature Biotech.* **24**, pp. 848–51, 2006.

7. X. Wang, Y. Pang, G. Ku, X. Xie, G. Stoica, and L.-H. Wang, "Non-invasive laser-induced photoacoustic tomography for structural and functional imaging of the brain *in vivo*," *Nature Biotech.* **21**, pp. 803–6, 2003.
8. R. A. Kruger, W. L. Kiser Jr., D. R. Reinecke, G. A. Kruger, and K. D. Miller, "Thermoacoustic optical molecular imaging of small animals," *Molecular Imaging* **2**, pp. 113–23, 2003.
9. R. I. Siphanto, K. K. Thumma, R. G. M. Kolkman, T. G. van Leeuwen, F. F. M. de Mul, J. W. van Neck, L. N. A. van Adrichem, and W. Steenbergen, "Serial noninvasive photoacoustic imaging of neovascularization in tumor angiogenesis," *Opt. Express* **13**, pp. 89–95, 2005.
10. J. C. Bamber, "Acoustical characteristics of biological media," in *Encyclopedia of Acoustics*, M. J. Crocker, ed., ch. 141, pp. 1703–26, John Wiley, New York, 1997.
11. R. G. M. Kolkman, W. Steenbergen, and T. G. Van Leeuwen, "Reflection mode photoacoustic measurement of speed of sound," *Opt. Express* **in print**, 2007.
12. X. Jin and L.-V. Wang, "Thermoacoustic tomography with correction for acoustic speed variations," *Phys. Med. Biol.* **51**, pp. 6437–6448, 2006.
13. Y. Xu, M. Xu, and L.-H. Wang, "Exact frequency-domain reconstruction for thermoacoustic tomographyii: Cylindrical geometry," *IEEE Trans. Med. Imaging* **21**, pp. 829–33, 2002.
14. R. A. Kruger, W. L. Kiser Jr., K. D. Miller, H. E. Reynolds, D. R. Reinecke, G. A. Kruger, P. J. Hofacker, and R. L. Eisenhart, "Thermoacoustic CT scanner for breast imaging: Design considerations," in *Biomedical Optoacoustics III*, K. K. Shung and M. F. Insana, eds., *Proc. Soc. Photo-Opt. Instrum. Engg. (SPIE)* **3982**, pp. 354–9, 2000.
15. C. G. A. Hoelen and F. F. M. de Mul, "Image reconstruction for photoacoustic scanning of tissue structures," *Appl. Opt.* **39**, pp. 5872–83, 2000.
16. S. J. Norton and M. Linzer, "Ultrasonic reflectivity tomography: reconstruction with circular transducer arrays," *Ultrason. Imaging* **1**, pp. 154–84, 1979.
17. A. Kak and M. Slaney, *Principles of Computerized Tomographic Imaging*, IEEE Press, New York, 1988.